Extended Data Figure 1

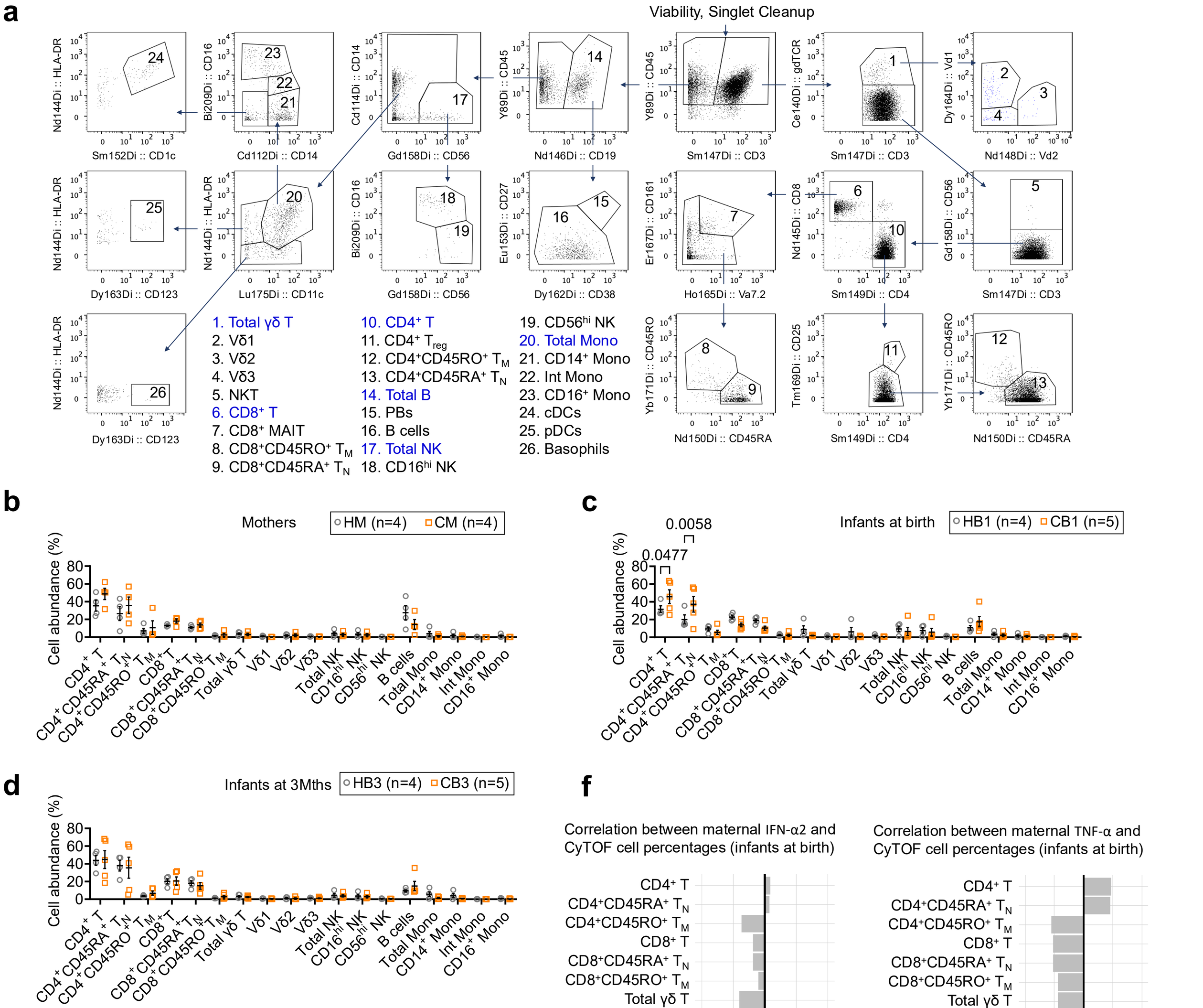

Extended Data Fig. 1: CyTOF cell abundance and plasma cytokine/chemokine levels in mother-infant dyads

a, Cytometry dot plots showing the gating strategy in CyTOF analysis for the characterization of 26 cell types, including 6 major cell types (blue text) and 20 minor cell types (black text).

b-**d**, Scatter plots of CyTOF cell abundance in mothers (**b**), infants at birth (**c**), and infants at 3-month of life (**d**). Error bars denote mean ± SEM. $p<0.05$, two-way ANOVA test with Šidák's multiple comparisons test.

e, H&E staining of placenta slides from healthy, and COVID-19 mother. Areas of inflammation are indicated by arrows. Scale bar represents 50mm.

f, Double-sided bar plots showing rho values (x-axis) of Spearman's correlation between maternal IFN-α2 (left) and TNF-α (right) levels with the corresponding immune cell percentages (CyTOF data) in paired infant at birth. $p<0.05$ are labelled.

g, Spearman's correlation plot between maternal TNF-α plasma concentrations and B cell percentages in infants at birth. Linear regression line and area of 95% confidential interval are shown.

h, PCA plot of plasma cytokine/chemokine concentrations of individual samples.

i, Spearman's correlations between plasma IL-7 concentrations and $CD4^+CD45RO^+$ T_M (left) and $CD8^+CD45RA^+$ T_N (right) cell percentages in infants at birth. Linear regression line and area of 95% confidential interval are shown.

Extended Data Figure 2

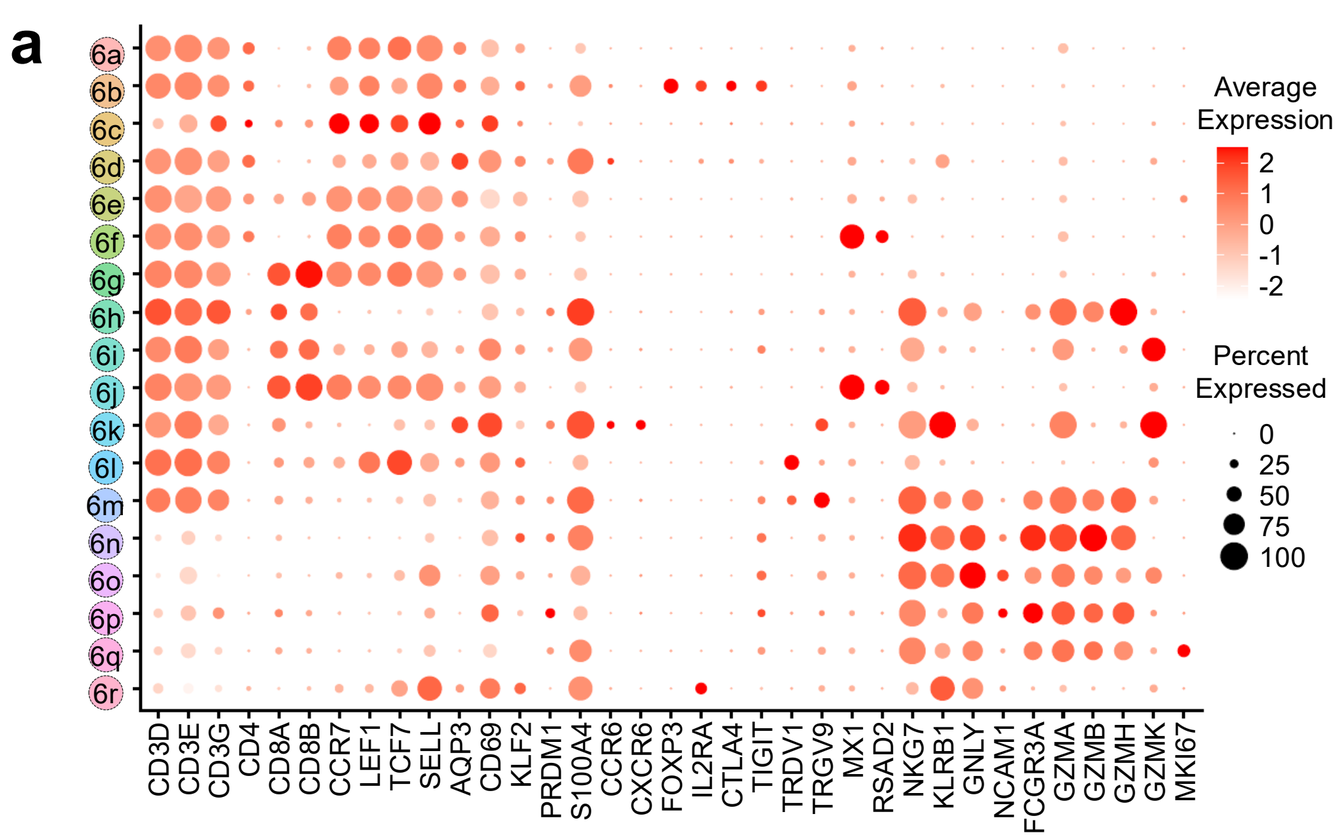

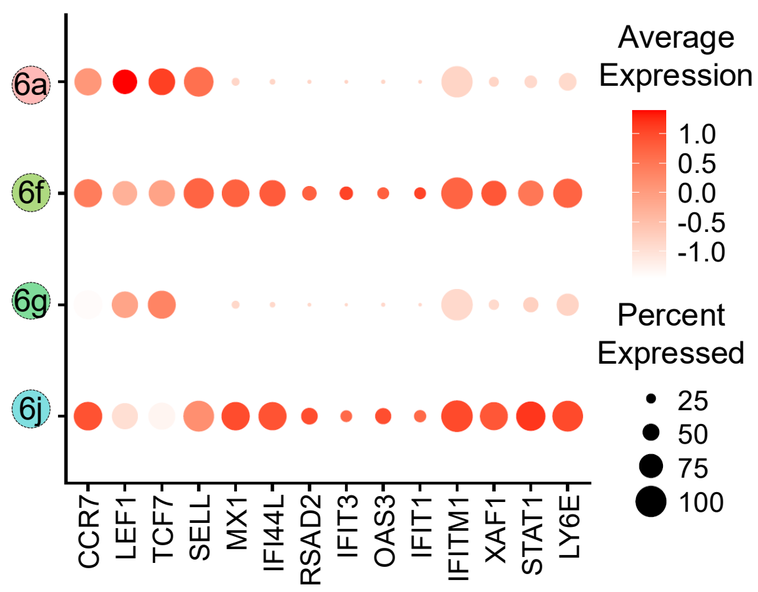

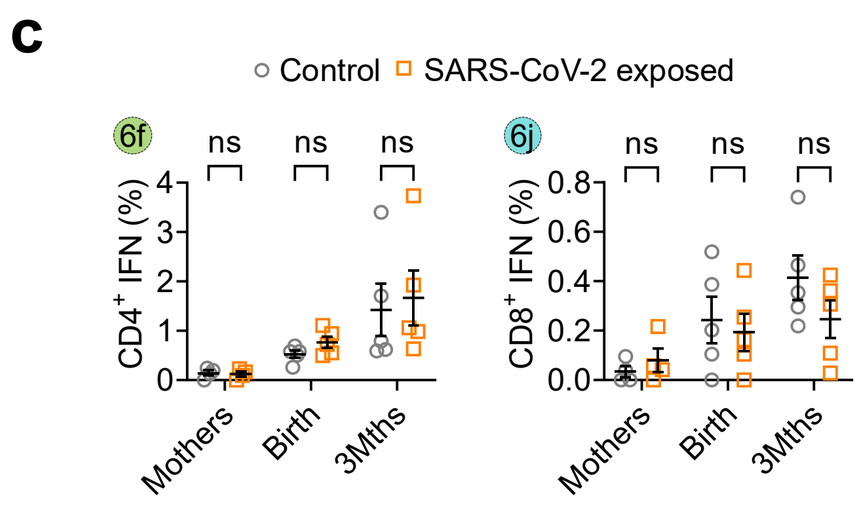

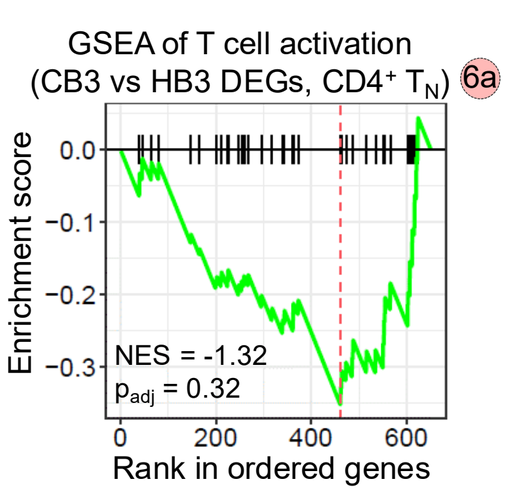

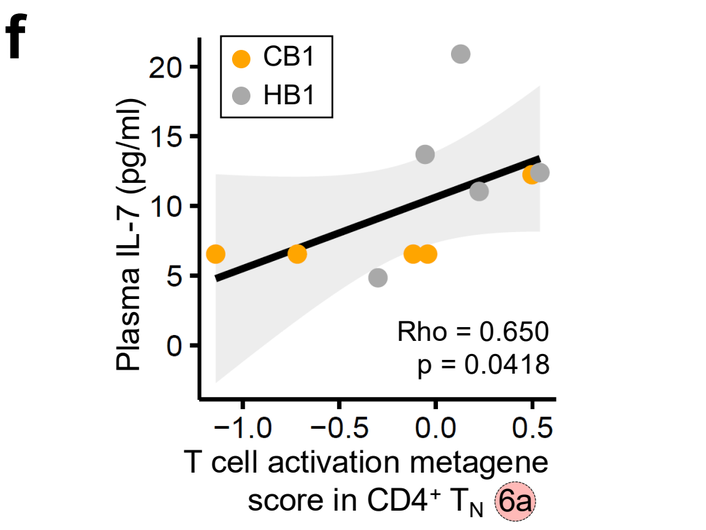

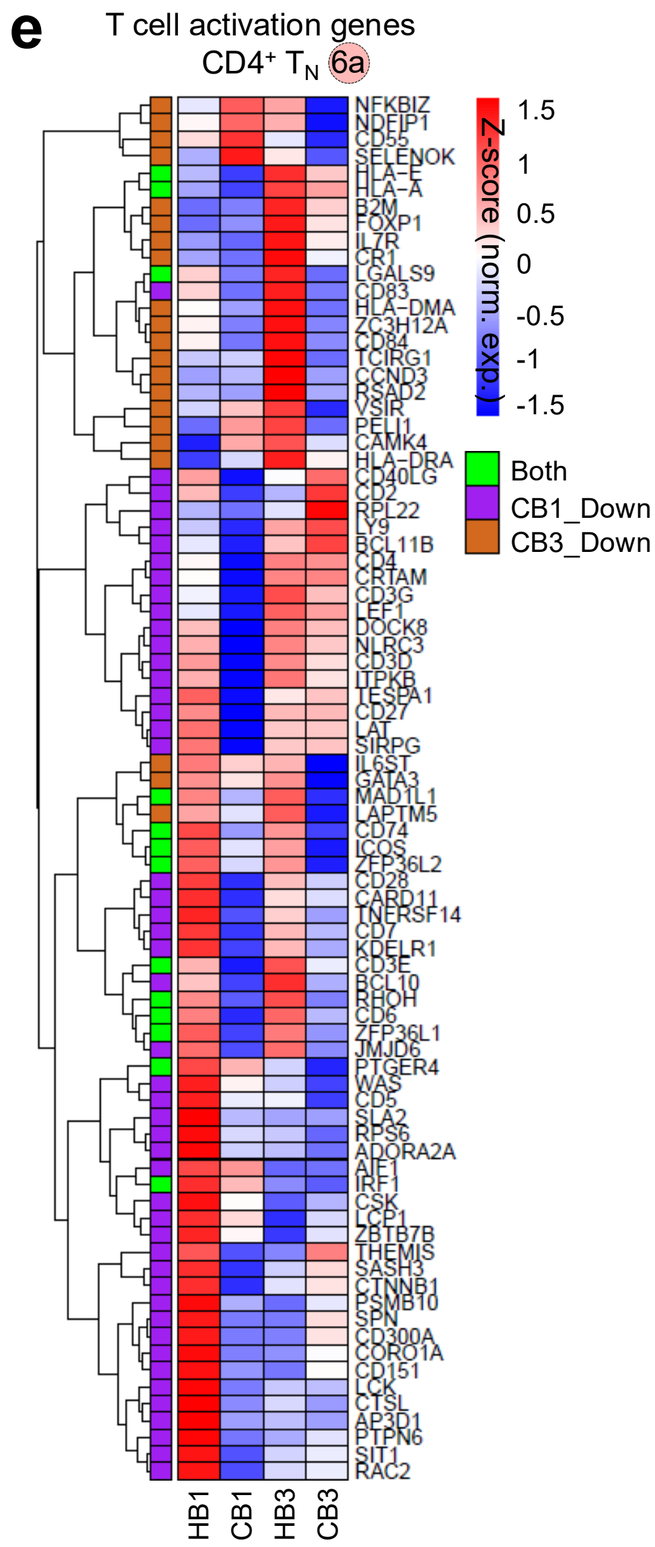

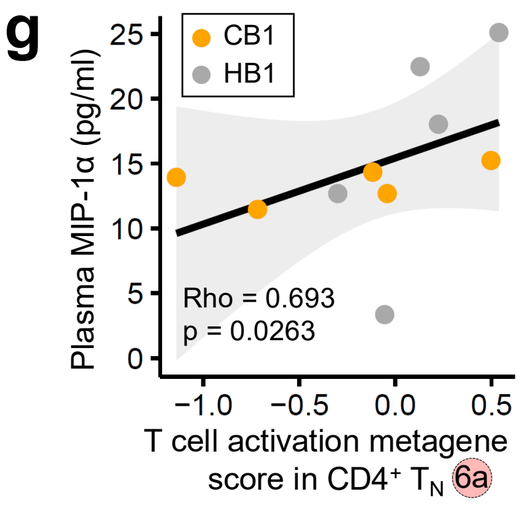

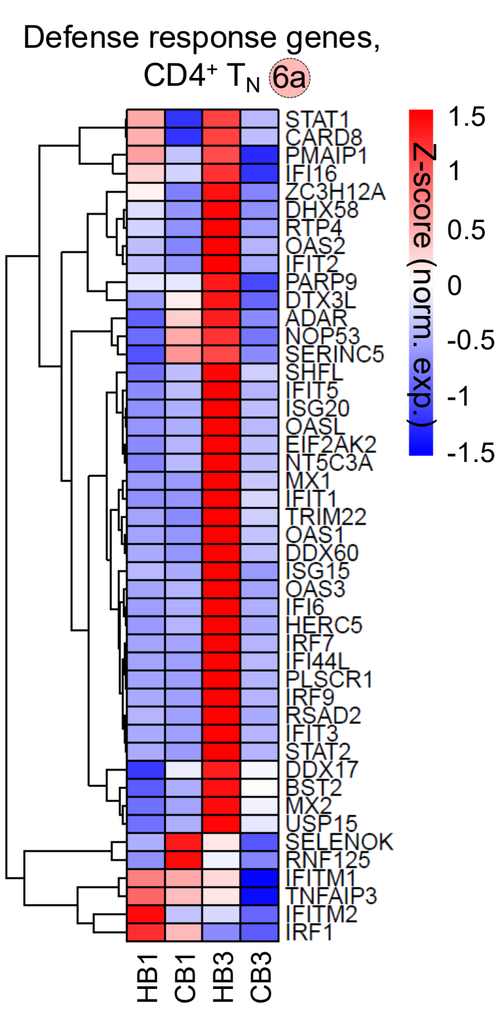

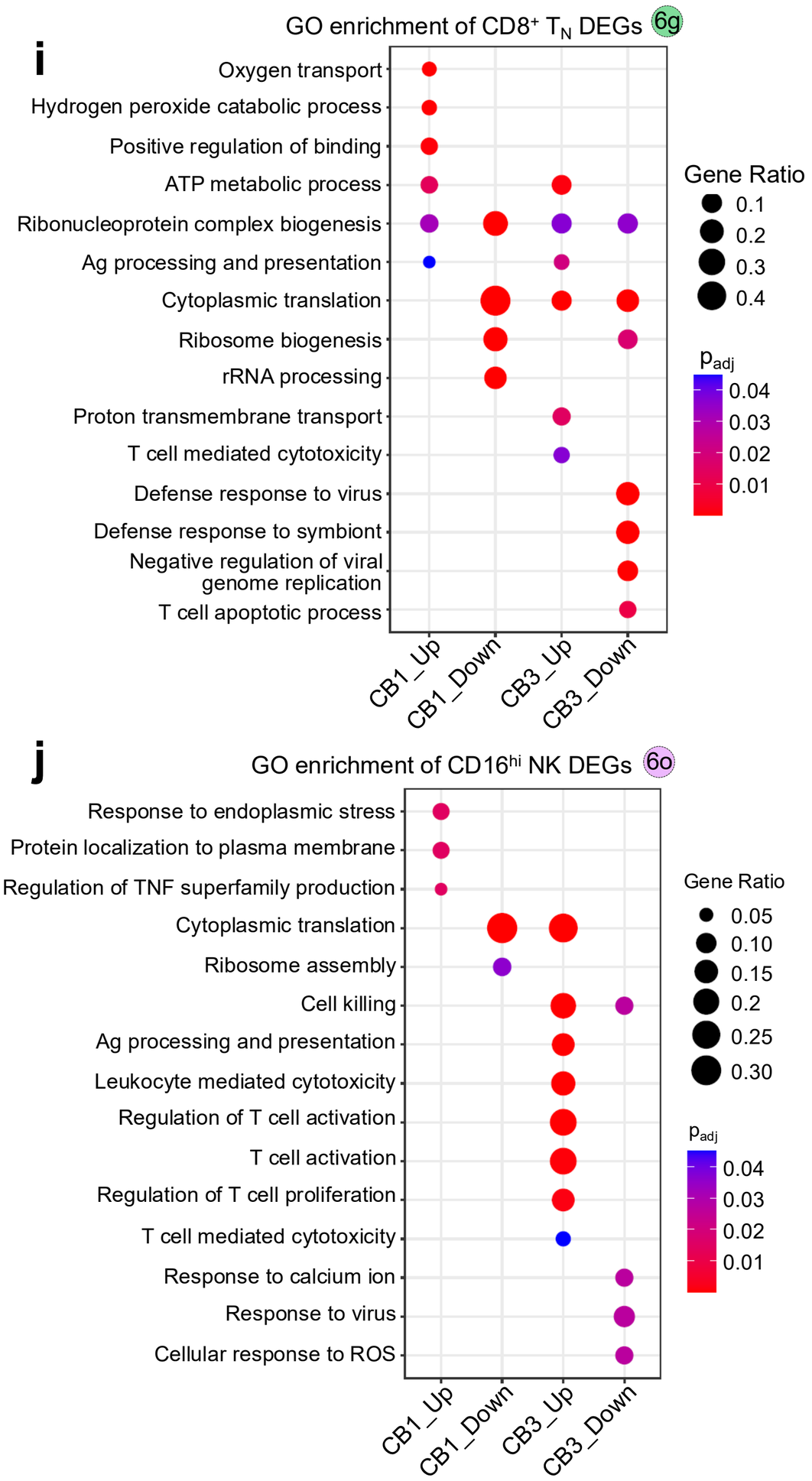

Extended Data Fig. 2: Characterization of NK and T cell subtypes in scRNA-seq

a, Bubble plot showing gene expression of known cell type markers in NK and T cell subtypes. Colors and bubble sizes represent the mean normalized expression and percentage of cells expressing the genes, respectively.

b, Bubble plot showing gene expression of T_N cell markers (CCR7, LEF1, TCF7, SELL) and ISGs in $CD4^+$ T_N (6a), $CD4^+$ IFN (6f), $CD8^+$ T_N (6g), and $CD8^+$ IFN (6j) cells.

c, Percentages of $CD4^+$ IFN (left) and $CD8^+$ IFN (right) cells in all NK and T cells. Error bars denote mean ± SEM. $p<0.05$, two-way ANOVA test with Šidák's multiple comparisons test; ns: not significant.

d, GSEA plot of T cell activation using $CD4^+$ T_N DEGs in CB3 vs HB3. Normalized enrichment score (NES) and adjusted p-value are indicated.

e, Heatmap of $CD4^+$ T_N DEGs involved in T cell activation GO. K-means clusters of genes are shown. Colored boxes on the left of the heatmap represent the category of DEGs, including CB1_Down (purple), CB3_Down (orange), and both (green).

f-g, Spearman's correlation between the T cell activation metagene score in CD4 T_N (scRNA-seq data) at birth with plasma IL-7 (**f**) or MIP-1α (**g**). Linear regression line and area of 95% confidential interval are shown.

h, Heatmap of $CD4^+$ T_N DEGs (CB3_Down) involved in viral response GO. K-means clusters of genes are shown.

i-j, GO terms enriched in $CD8^+$ T_N (**j**) and $CD16^{hi}$ NK (**k**) in DEGs (CB1_Up: up-regulated genes in CB1 vs HB1; CB1_Down: down-regulated genes in CB1 vs HB1; CB3_Up: up-regulated genes in CB1 vs HB1; CB3_Down: down-regulated genes in CB3 vs HB3).

Extended Data Figure 3

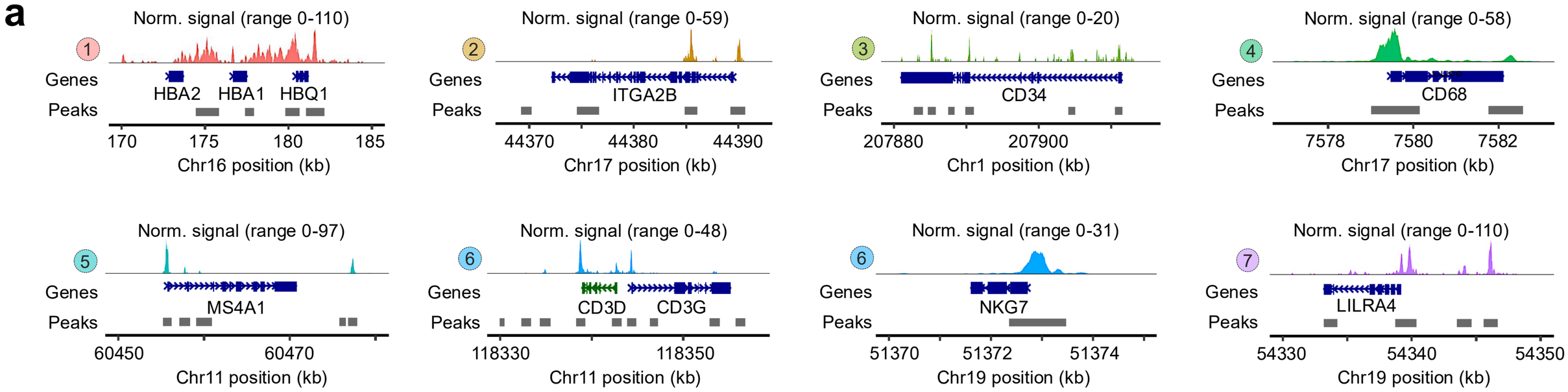

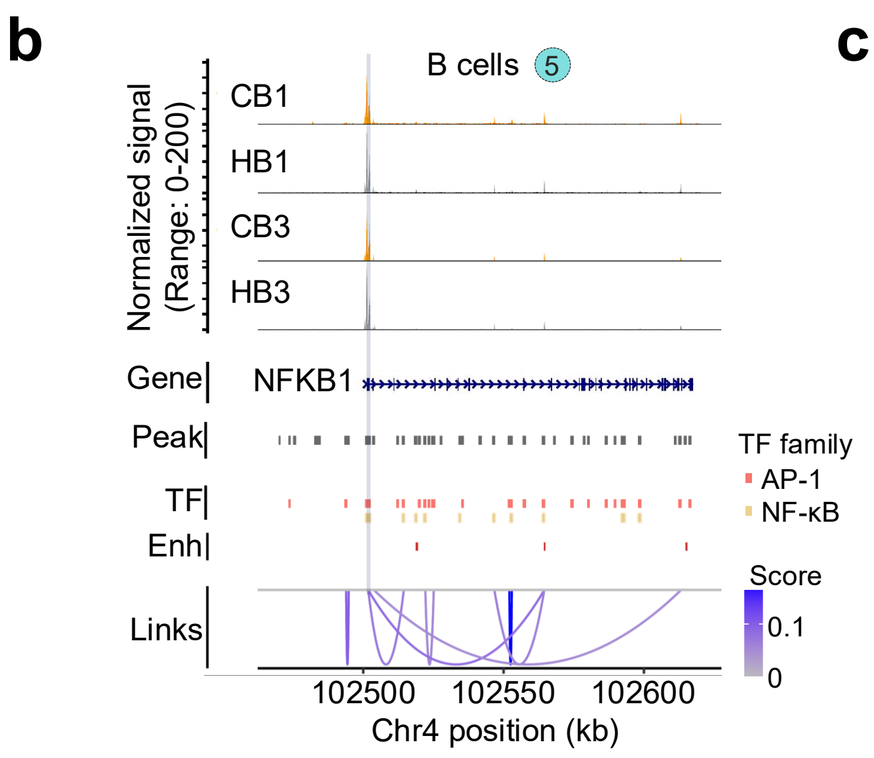

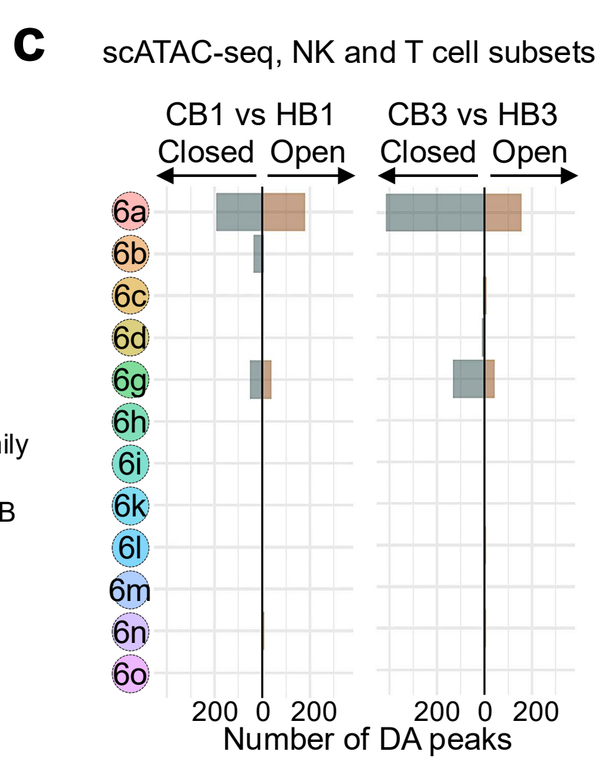

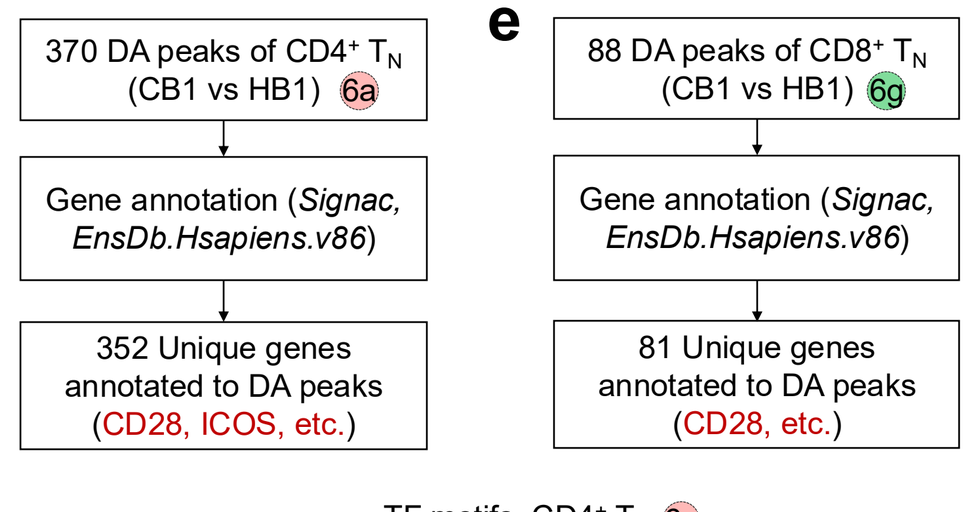

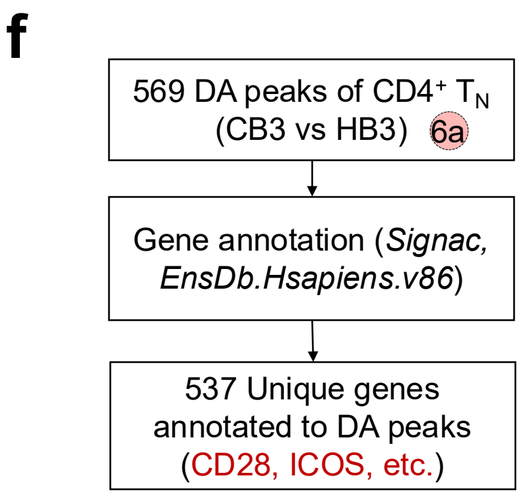

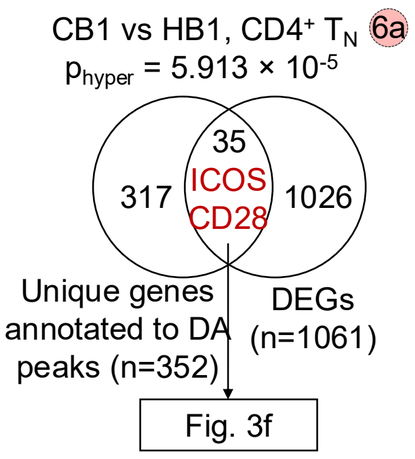

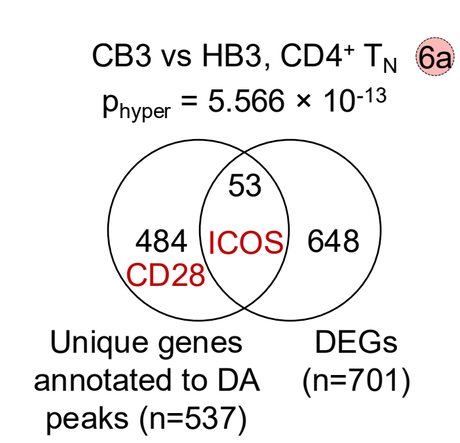

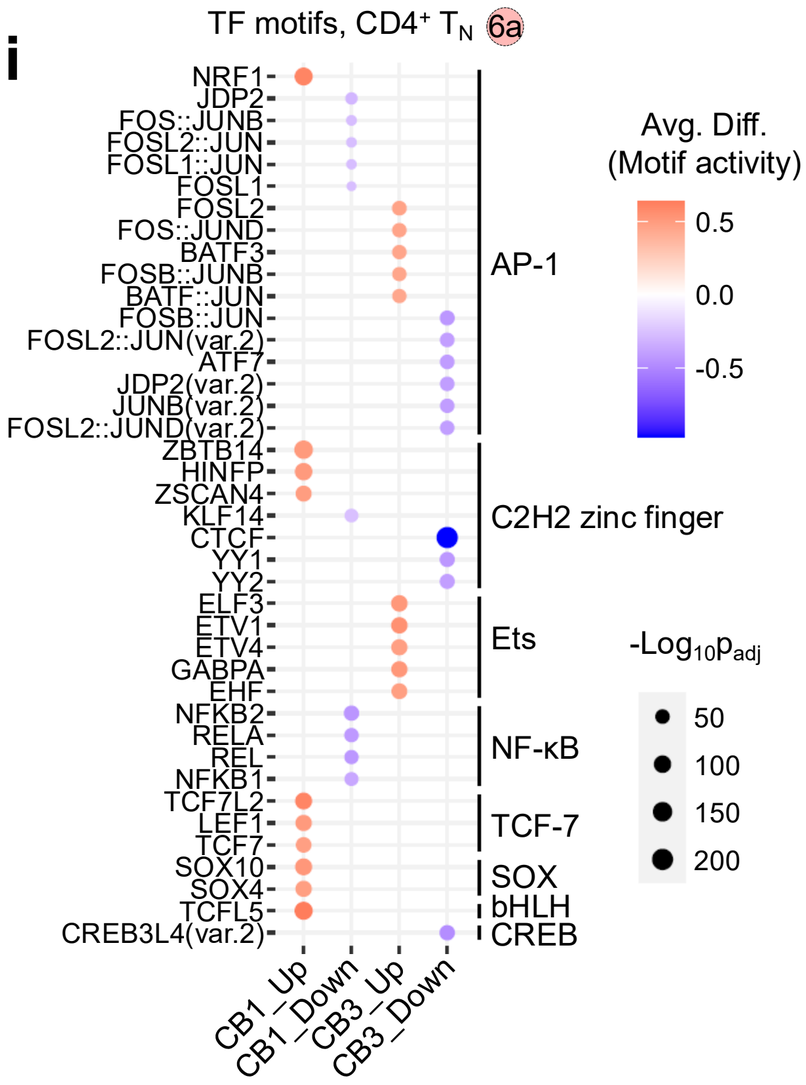

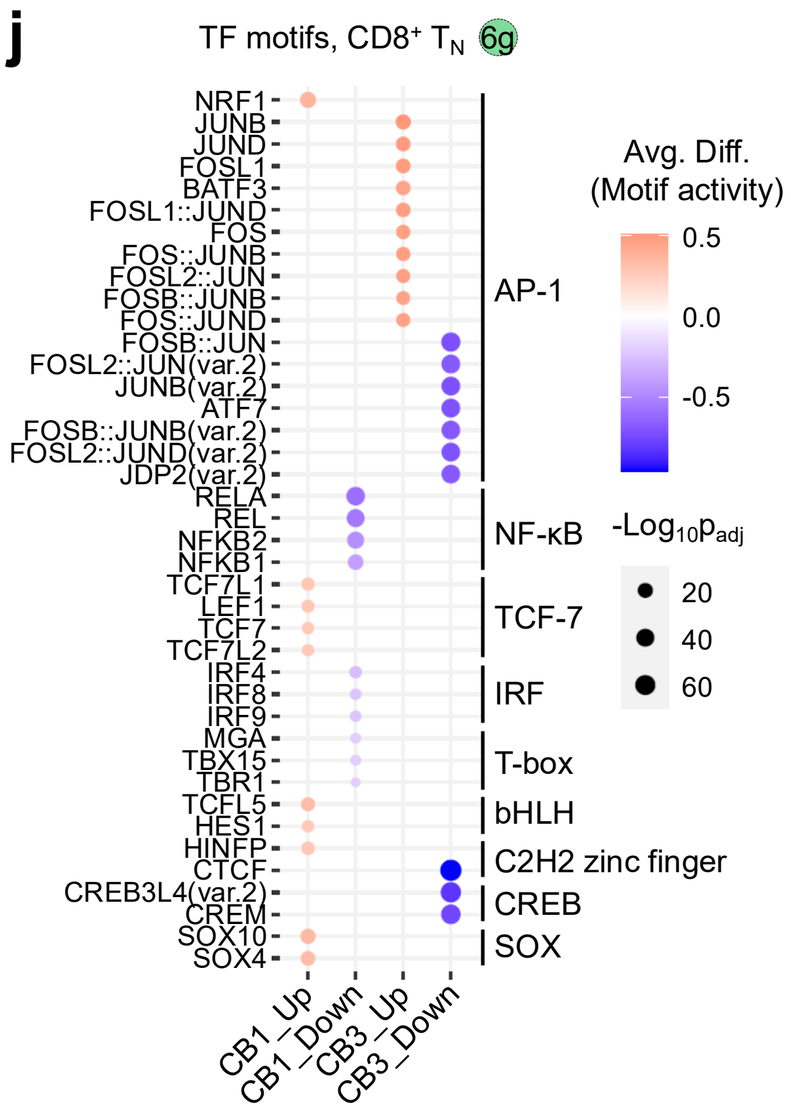

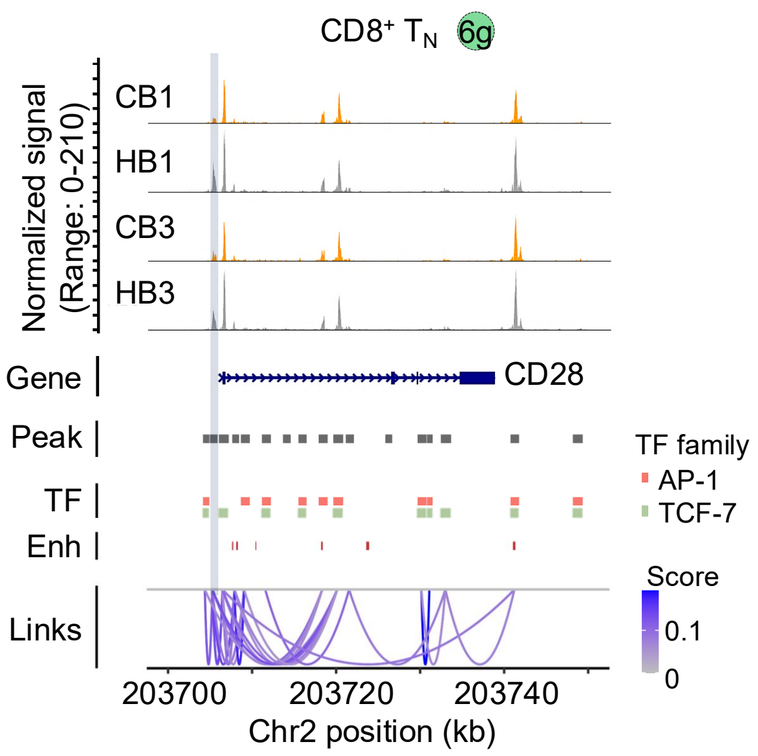

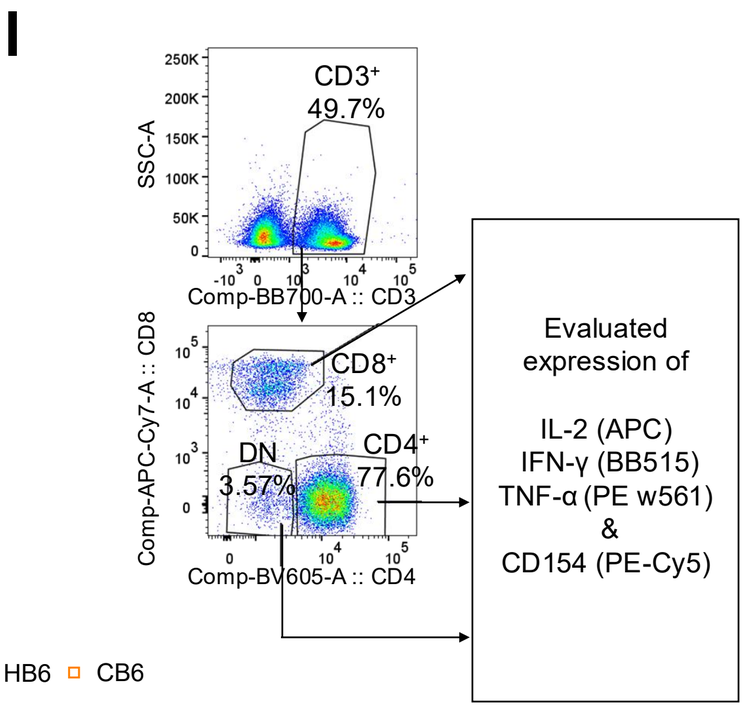

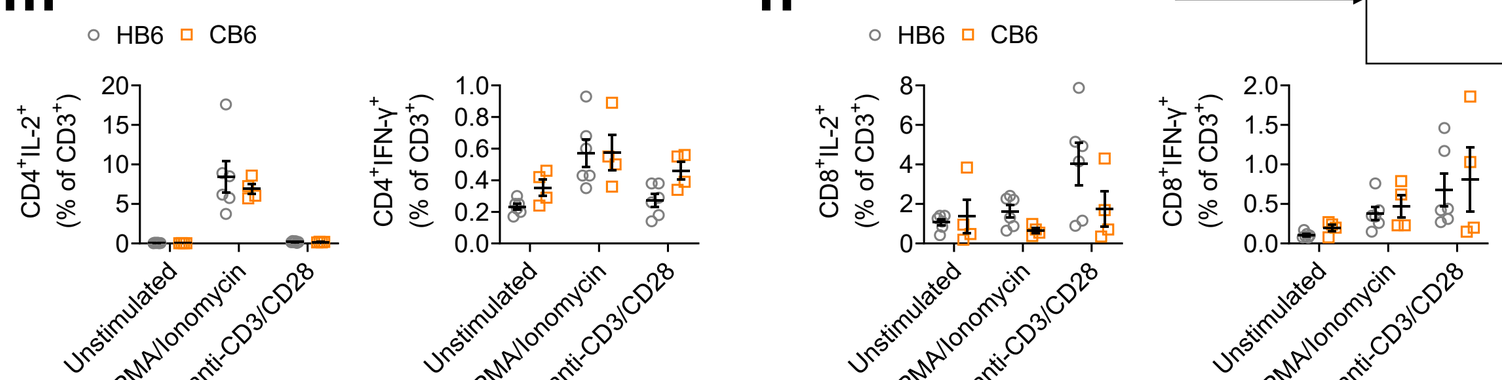

Extended Data Fig. 3. Single-cell chromatin accessibility profiling and T cell functional assays

a, Genomic view (hg38, Coverage plots) of canonical cell type markers in 7 major cell types of scATAC-seq data.

b, Genomic view showing chromatin accessibility of infant B cells at NFKB1 locus. A DA peak in CB3 vs HB3 is highlighted in light grey shade. Peaks containing motifs of AP-1 (red) and NF-κB (yellow) TF families from ENCODE project. The links track shows *cis*-regulatory elements interactions predicted by co-accessibility algorithm.

c, Double-sided bar plots showing the number of DA peaks between CB1 vs HB1 and CB3 vs HB3 in NK and T cell subsets.

d, Schematic of gene annotation of DA peaks (CB1 vs HB1) in $CD4^+$ T_N.

e, Schematic of gene annotation of DA peaks (CB3 vs HB3) in $CD4^+$ T_N.

f, Schematic of gene annotation of DA peaks (CB1 vs HB1) in $CD8^+$ T_N.

g, Venn diagram showing the overlapping results between unique genes annotated to DA peaks (CB1 vs HB1) and DEGs (CB1 vs HB1) in $CD4^+$ T_N. p-values <0.05, hypergeometric test.

h, Venn diagram showing the overlapping results between unique genes annotated to DA peaks (CB3 vs HB3) and DEGs (CB3 vs HB3) in $CD4^+$ T_N. p-values <0.05, hypergeometric test.

i-j, Bubble plot of top 10 TFs with differential motif activity scores in $CD4^+$ T_N (**i**) and $CD8^+$ T_N (**j**) of SEU and healthy infants. Colors and bubble sizes represent the average difference in motif activity and $-\log_{10}$ of adjusted p-values, respectively. TF families are labelled on the right.

k, Genomic view showing chromatin accessibility of infant $CD8^+$ T_N at CD28 locus. A DA peak in CB1 vs HB1 is highlighted in light grey shade. Peaks containing motifs of AP-1 (red) and TCF-7 (green) TF families from ENCODE project. The links track shows *cis*-regulatory elements interactions predicted by co-accessibility algorithm.

l, Flow cytometry dot plots showing the gating strategy in the analysis of *ex vivo* T cell responses.

m-**n**, Percentages of $CD4^+$ T cells (**m**) and $CD8^+$ T cells (**n**) producing intracellular IL-2 (left) and IFN-γ (right) upon *ex vivo* stimulation. Error bars denote mean ± SEM. None of the comparisons had $p<0.05$, two-way ANOVA test with Šidák's multiple comparisons test.

Extended Data Figure 4

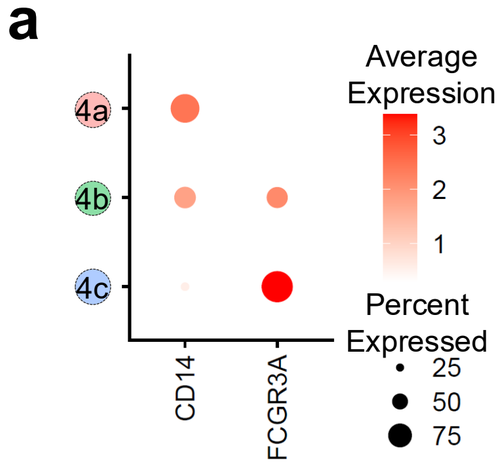

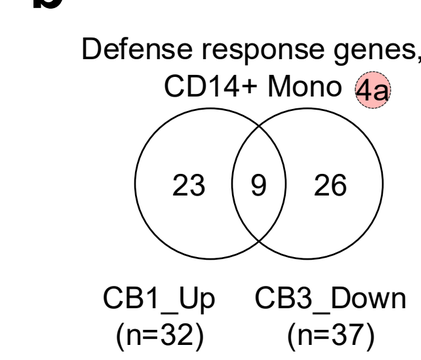

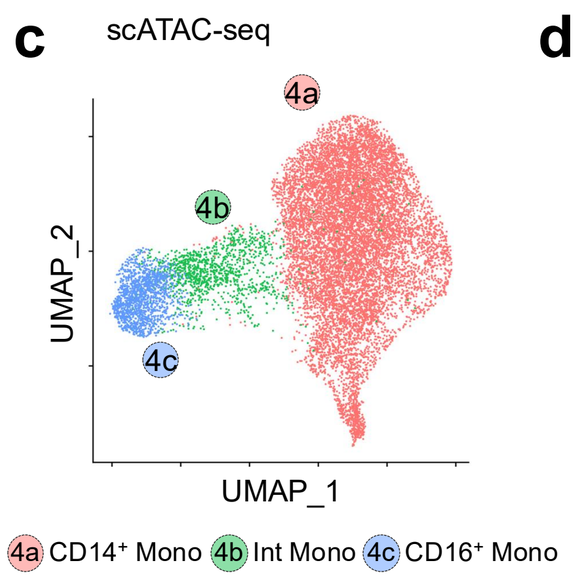

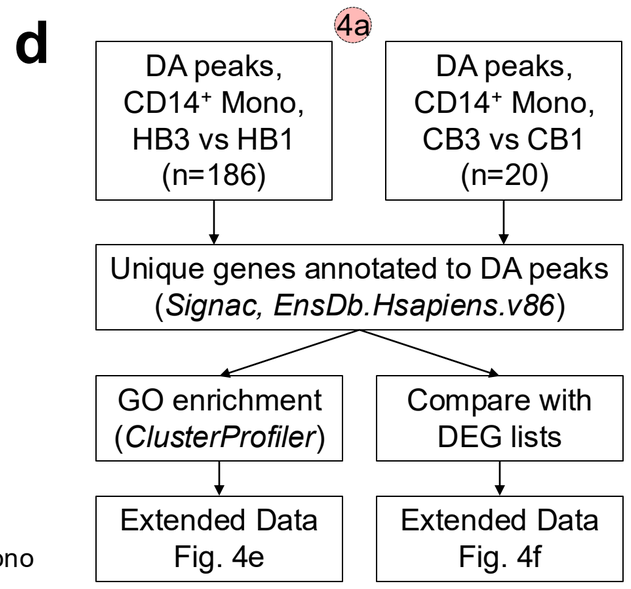

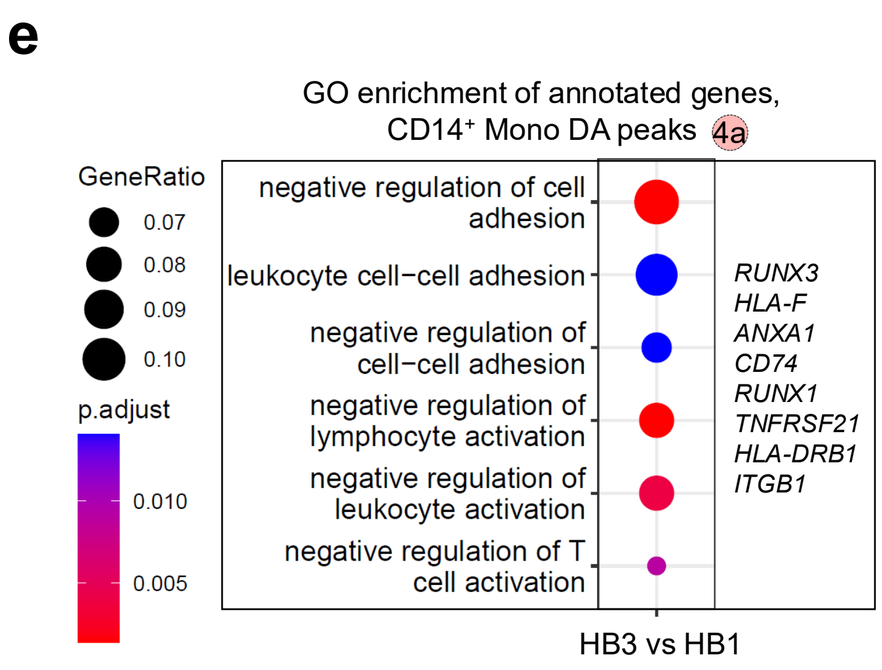

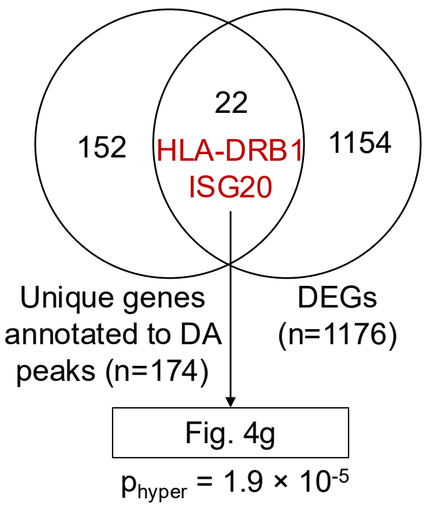

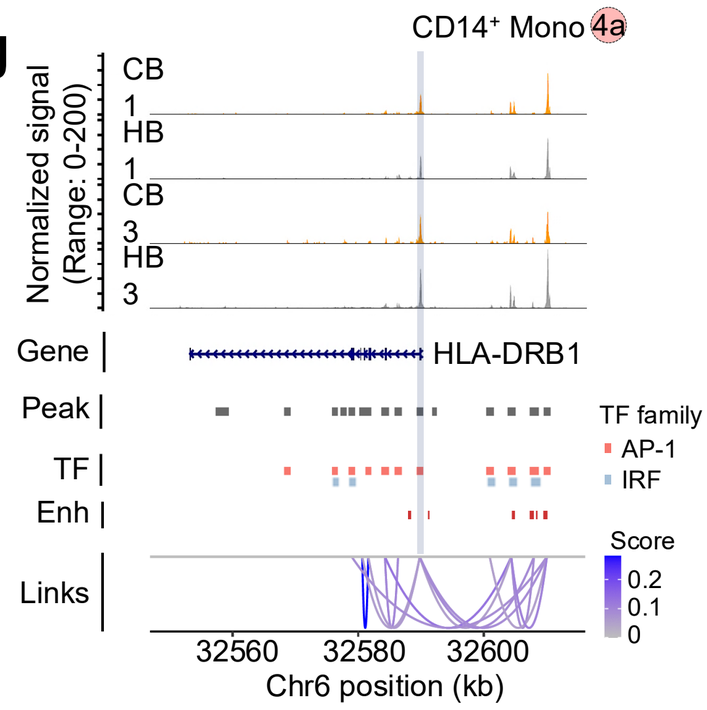

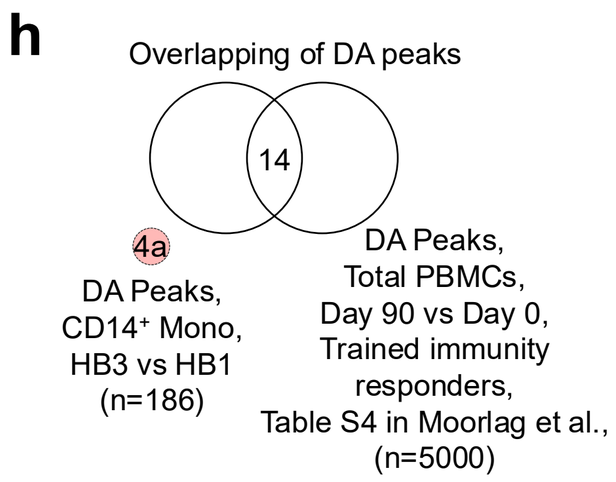

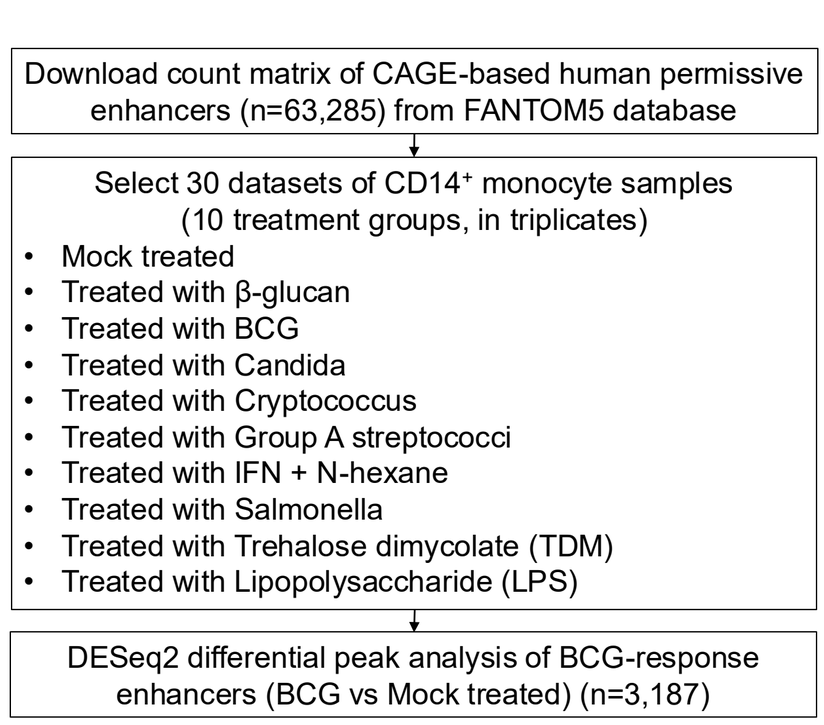

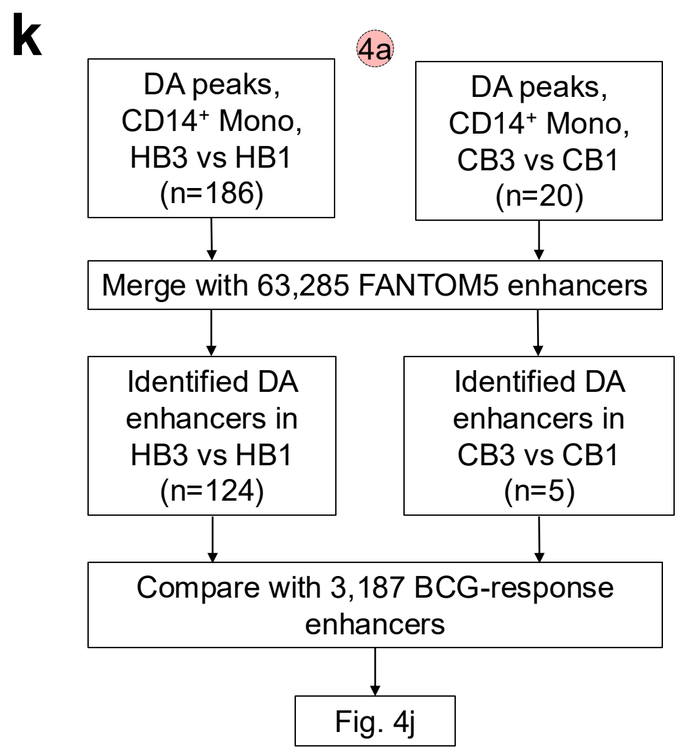

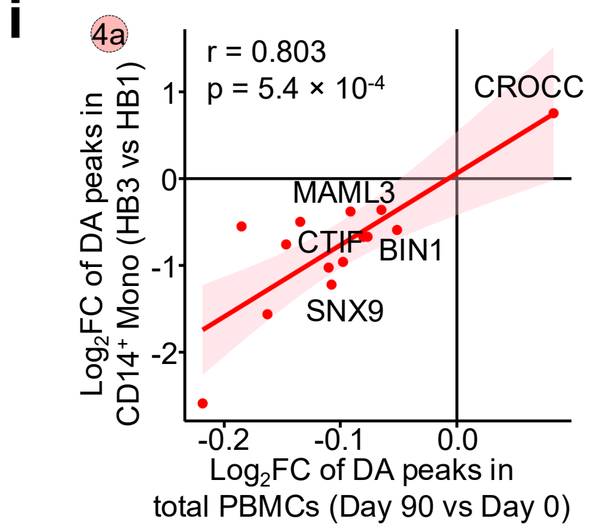

Extended Data Fig. 4: Longitudinal analysis of CD14⁺ monocytes chromatin accessibility and enhancers in infants

a, Bubble plot showing gene expression of known cell type markers in monocyte subtypes.

b, Venn diagram showing the overlapping results between CB1_Up and CB3_Down DEGs involved in defense response GO terms enriched in CD14⁺ monocytes.

c, UMAP plot of monocyte subsets in scATAC-seq data.

d, Schematic of gene annotation and downstream analysis of CD14⁺ monocyte DA peaks between infants at 3-month and birth.

e, GO terms enriched in genes annotated to CD14⁺ monocyte DA peaks (HB3 vs HB1).

f, Venn diagram showing the overlapping results between unique genes annotated to DA peaks (HB3 vs HB1) and DEGs (HB3 vs HB1) in CD14⁺ monocytes. $p<0.05$, hypergeometric test.

g, Genomic view showing chromatin accessibility of infant CD14⁺ monocytes at HLA-DRB1 locus. A DA peak in HB3 vs HB1 is highlighted in light grey shade. Peaks containing motifs of AP-1 (red) and IRF (blue) TF families from ENCODE project. The links track shows *cis*-regulatory elements interactions predicted by co-accessibility algorithm.

h, Venn diagram showing the overlapping results between DA peaks (HB3 vs HB1) in CD14⁺ monocytes and DA peaks (Day 90 vs Day 0) in total PBMCs of trained immunity responders identified by Moorlag et al.

i, Pearson correlation of DA peaks (HB3 vs HB1) in CD14⁺ monocytes overlapped with DA peaks (Day 90 vs Day 0) in total PBMCs of trained immunity responders identified by Moorlag et al. *Y*-axis and X-axis represent $\log_2$FC of chromatin accessibility in the two datasets respectively. Linear regression line and area of 95% confidential interval are shown.

j, Schematic of analyzing human permissive enhancers from FANTOM5 database. BCG-response enhancers were identified by comparing the enhancer expression in BCG and mock treated CD14⁺ monocytes. See Methods.

k, Schematic of analyzing DA enhancers in CD14⁺ monocytes from this study. DA enhancers between infants at 3-month and birth (HB3 vs HB1 and CB3 vs CB1) were obtained by merging CD14⁺ monocyte DA peaks with all human permissive enhancers in FANTOM5 database. The lists of DA enhancers were then compared to 3,187 BCG-response enhancers (from **j**).

Extended Data Figure 5

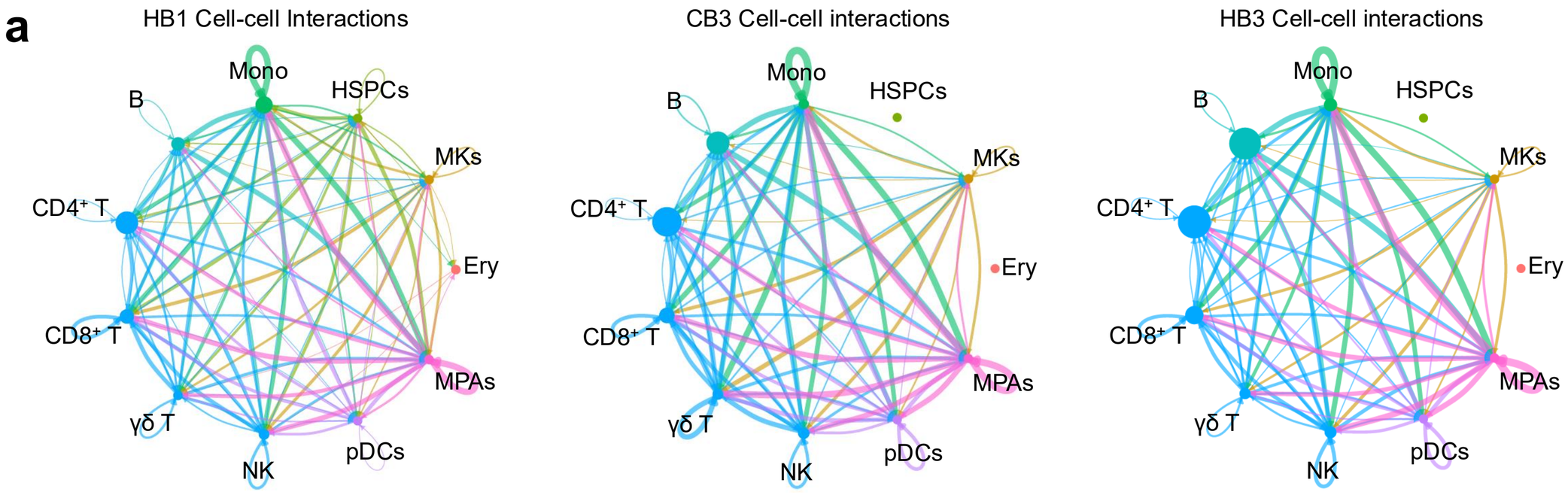

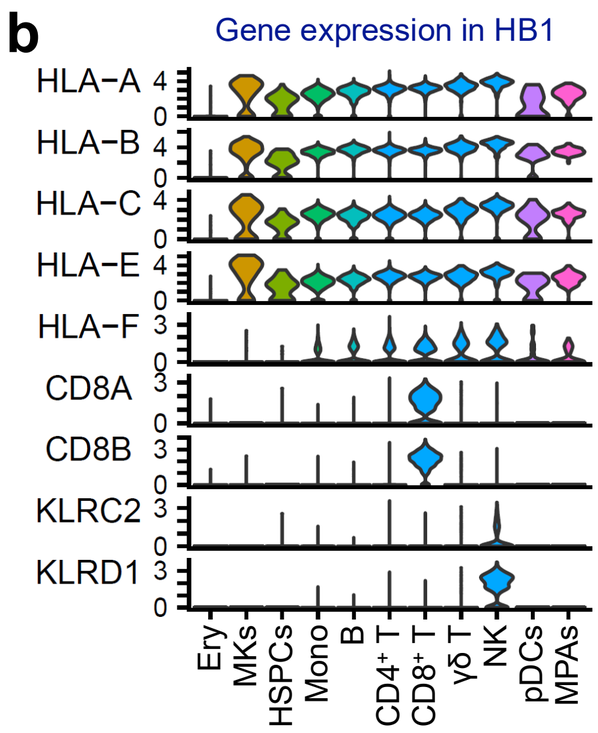

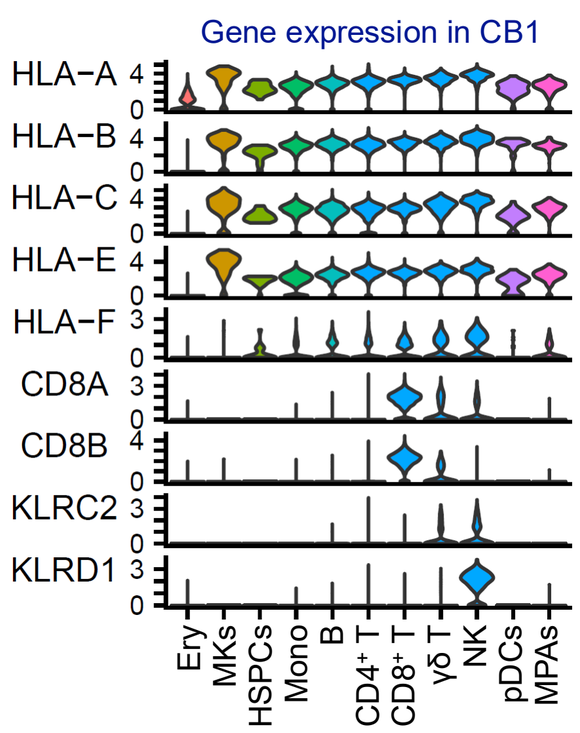

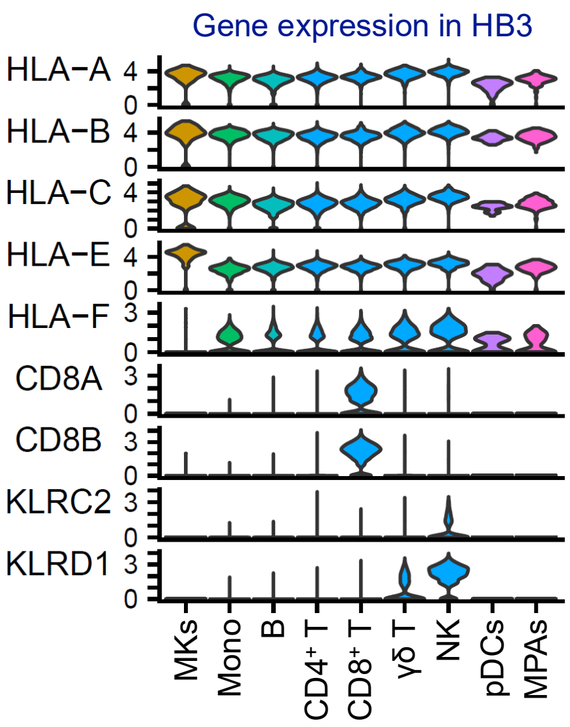

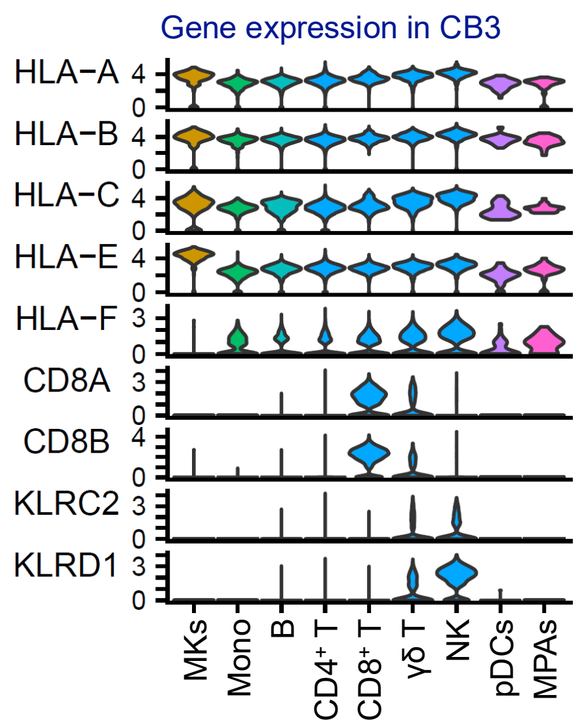

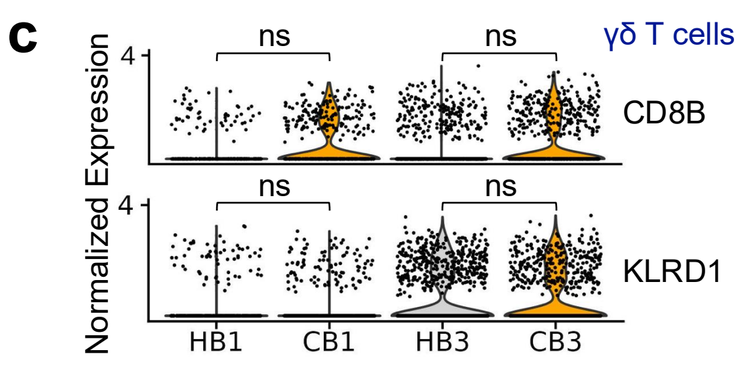

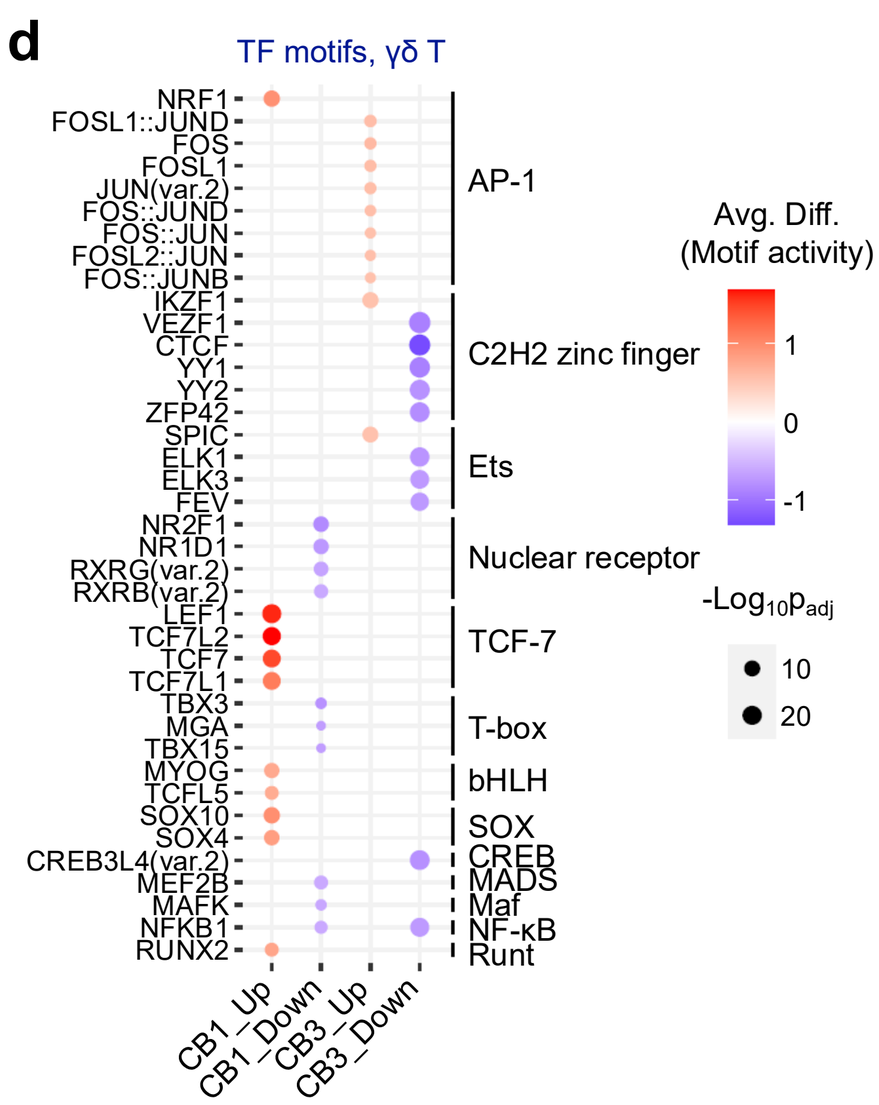

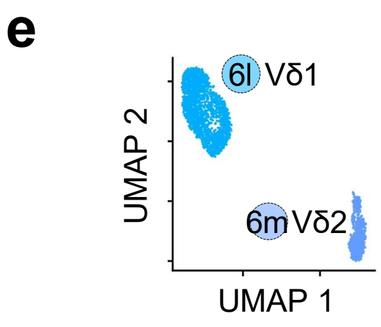

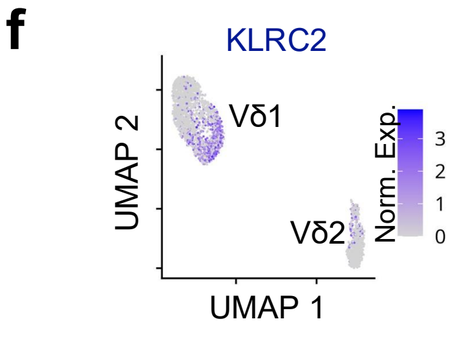

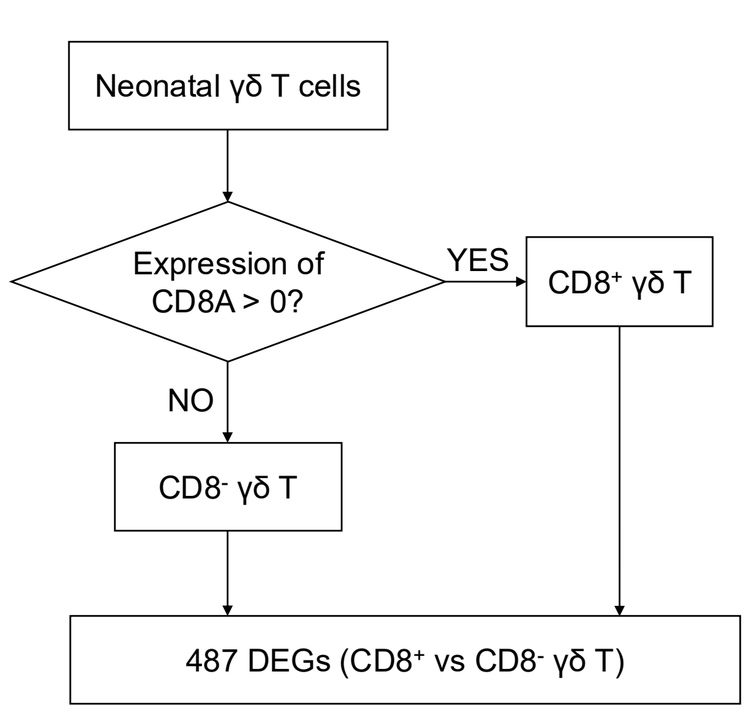

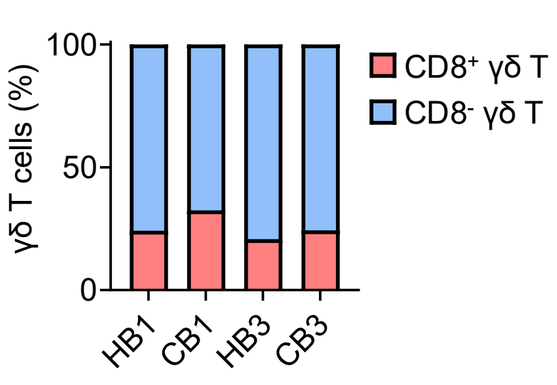

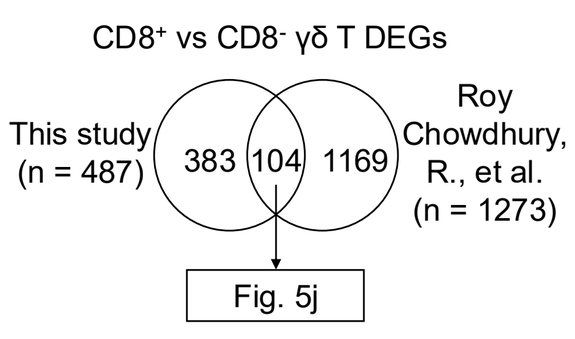

Extended Data Fig. 5: Cell-cell communications and characterization of infant γδ T cells

a, Circle plots of cell-cell communication networks among 11 main cell groups in HB1 (left), CB3 (middle), and HB3 (right). Colors denote the sourcing cell types of pairwise interactions. Vertex sizes and edge widths represent the number of cells in the cell group and the number of predicted interactions, respectively.

b, Violin plots of normalized gene expression of MHC-I signalling ligands and receptors in 11 cell groups of HB1 (top left), CB1 (top right), HB3 (bottom left), and CB3 (bottom right).

c, Violin plots of normalized gene expression of CD8B and KLRD1 (CD94) in infant γδ T cells. p_{adj}<0.05 (CB1 vs HB1 or CB3 vs HB3), Wilcoxon rank-sum test with Bonferroni correction; ns: not significant.

d, Bubble plot of top 10 TFs with differential motif activity scores in γδ T cells of SEU and healthy infants. TF families are labelled on the right.

e, UMAP plot of re-clustered infant γδ T cells in scRNA-seq data. Vδ1 and Vδ2 are labelled.

f, Feature plot showing gene expression of KLRC2 in infant γδ T cells. Colors denote normalized gene expression.

g, Schematic of characterization of $CD8^+$ and $CD8^-$ cell states of neonatal γδ T based on CD8A gene expression.

h, Stacked bar plot showing percentages of $CD8^+$ (pink) and $CD8^-$ (skyblue) cell states in all γδ T cells of SEU and healthy infants.

i, Venn diagram showing the overlapping results between neonatal γδ T DEGs ($CD8^+$ vs $CD8^-$) and DEGs identified by Roy Chowdhury, et al.

Extended Data Figure 6

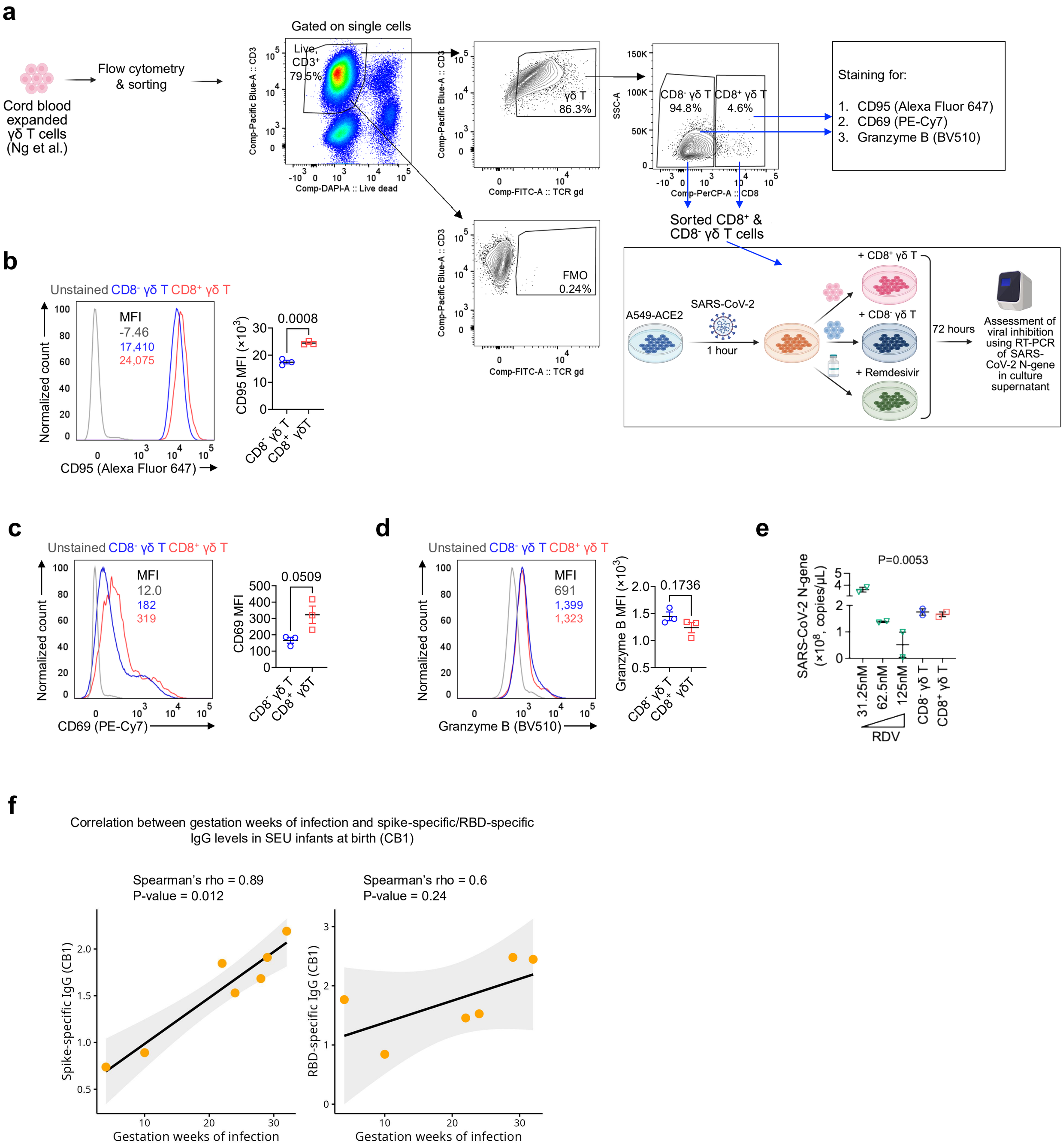

Extended Data Fig. 6: Cord blood expanded γδ T cell profiling and SARS-CoV-2 specific antibodies in infants

a, Gating strategy in flow cytometry of cord blood expanded γδ T cells and schematic of viral inhibition assay using sorted $CD8^+$ and $CD8^-$ γδ T cells.

b-d, Representative histograms (left) and dot plots (right) of CD95 (**b**), CD69 (**c**), and granzyme B (**d**) MFI in $CD8^+$ (red) and $CD8^-$ (blue) γδ T cells. Error bars in dot plots denote mean ± SEM. Two-sided unpaired *t*-test p-values are labelled.

e, Viral genome copy number in SARS-CoV-2 infected A549-hACE2 cells treated with Remdesivir at various doses or co-cultured with $CD8^+$ or $CD8^-$ γδ T cells. $p<0.05$, Kruskal-Wallis test.

f, Spearman's correlation between spike-specific and RBD-specific IgG levels at birth and maternal infection time. Linear regression lines and areas of 95% confidential interval are shown.